A Fast Higher-Order Time-Domain Finite Element-Boundary Integral Method for 3-D Electromagnetic Scattering Analysis

Dan Jiao, *Member, IEEE*, A. Arif Ergin, Balasubramaniam Shanker, *Senior Member, IEEE*, Eric Michielssen, *Fellow Member, IEEE*, and Jian-Ming Jin, *Fellow, IEEE*

***Abstract*—A novel hybrid time-domain finite element-boundary integral method for analyzing three-dimensional (3-D) electromagnetic scattering phenomena is presented. The method couples finite element and boundary integral field representations in a way that results in a sparse system matrix and solutions that are devoid of spurious modes. To accurately represent the unknown fields, the scheme employs higher-order vector basis functions defined on curvilinear tetrahedral elements. To handle problems involving electrically large objects, the multilevel plane-wave time-domain algorithm is used to accelerate the evaluation of the boundary integrals. Numerical results demonstrate the accuracy and versatility of the proposed scheme.**

***Index Terms*—Electromagnetic scattering, finite-element method, higher-order method, transient analysis.**

I. Introduction

THE HYBRID finite element-boundary integral (FE-BI) method is a powerful numerical technique for solving open-region electromagnetic scattering problems. The method uses an artificial boundary to divide the infinite solution domain into interior and exterior regions in which fields are represented using finite elements (FEs) and boundary integrals (BIs), respectively. These two representations are coupled at the artificial boundary by enforcing field continuity. The resulting scheme permits the accurate and efficient analysis of complex electromagnetic phenomena, especially those involving inhomogeneous media. This method was initially developed to solve two-dimensional (2-D) and three-dimensional (3-D) frequency-domain electromagnetic scattering problems (see [1] and references therein); here, its time-domain extension is considered.

Recently, considerable research efforts have been expended on the development of numerical techniques that allow electromagnetic phenomena to be modeled directly in the time domain, as these techniques permit the generation of wide-band data and the modeling of nonlinear materials. Undoubtedly, the best known technique for analyzing transient electromagnetic phenomena is the finite-difference time-domain (FDTD) method [2]. Other methods, however, have been gaining popularity. For example, recently, considerable progress has been reported on the development [3]–[6], stabilization [7]–[13] and acceleration [14]–[17] of time-domain integral equation solvers. In addition, a variety of time-domain FE schemes have been proposed [18]–[34]. One class of approaches directly solves Maxwell's equations [18]–[26]. These methods usually are explicit in nature, i.e., they do not require a matrix equation to be solved in each time step and operate in a leapfrog fashion similar to the FDTD method. Unfortunately, the well-developed frequency-domain FE method machinery does not apply to these schemes. Another class of time-domain FE solvers tackles the second-order vector wave equation, or the curl-curl equation, obtained by eliminating one of the field variables from Maxwell's equations [27]–[33]. The major disadvantage of these approaches is that they require the solution of a matrix equation at each time step.

An important issue in the finite-element solution of open-region scattering problems is the treatment of the artificial truncation boundary. One approach is to use an absorbing boundary condition (ABC), e.g., a perfectly matched layer (PML). However, unlike the FDTD method, techniques for implementing ABCs in time-domain FE schemes have received only scant attention [35], [36]. Another approach for truncating the boundary is to model exterior fields using a BI, which leads to the FE-BI method discussed earlier. This approach is numerically exact and more importantly, allows the truncation boundary to take on any shape (usually conformal to the object being studied) and to be placed close to the object, thereby minimizing the size of the computational domain. Although this approach has been thoroughly studied within the context of frequency domain solvers, it has not been explored extensively in a time-domain framework, except for relatively simple 2-D analysis [37], [38].

In this paper, we present a hybrid time-domain FE-BI method for analyzing 3-D electromagnetic open-region transient scattering phenomena. This work is an extension of a similar scheme that we developed for analyzing 2-D scattering problems [38]. This method has three unique features. The first is the hybridization scheme that combines the FE and BI representation of the fields. Instead of following the standard hybridization scheme used in the frequency domain, we propose a novel scheme that preserves the sparsity of the FE matrix and that yields solutions free of spurious modes associated with interior BI resonances.

Manuscript received November 20, 2000; revised August 6, 2001. This work was supported by AFOSR via the MURI program under Contract F49620-96-1-0025.

D. Jiao, A. A. Ergin, E. Michielssen, and J.-M. Jin are with the Center for Computational Electromagnetics, Department of Electrical and Computer Engineering, University of Illinois at Urbana-Champaign, Urbana, IL 61801-2991 USA.

B. Shanker is with the Department of Electrical and Computer Engineering, Iowa State University, Ames, IA 50010 USA.

Digital Object Identifier 10.1109/TAP.2002.801375

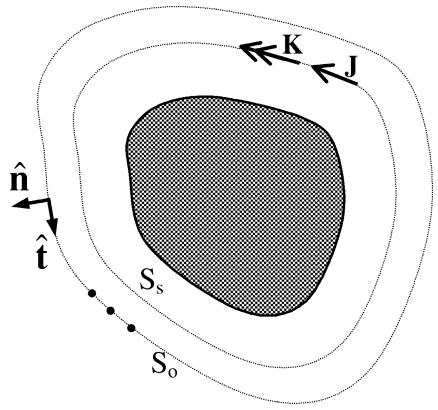

Fig. 1. Illustration of the truncation and source boundaries.

The second feature is the use of a fast algorithm, viz. the multilevel plane-wave time- domain (PWTD) method, for evaluating the BIs. Invoking this scheme greatly reduces the computational expense when an object of large electrical dimensions is considered. Third, the FE component of the solver employs curvilinear tetrahedral elements to precisely model the scatterer's geometry and higher-order vector basis functions to accurately represent the fields.

II. FE Formulation

This section describes the problem under consideration, the scheme to couple the FE and BI field representations and the numerical discretization adopted in the FE method.

A. Problem Statement and Hybridization Scheme

Consider the problem of modeling the electric field $\mathbf{E}$ generated by an external source in the presence of an object residing in a volume V_o. To formulate a FE scheme that permits computation of $\mathbf{E}$, we introduce an artificial surface S_o that encloses V_o (Fig. 1). Inside S_o, the field $\mathbf{E}$ satisfies

$$\nabla \times \left[\mu_r^{-1} \nabla \times \mathbf{E}(\mathbf{r},t)\right] + \mu_0 \epsilon \partial_t^2 \mathbf{E}(\mathbf{r},t) + \sigma \mu_0 \partial_t \mathbf{E}(\mathbf{r},t) = 0 \quad \mathbf{r} \in V_o. \tag{1}$$

For this equation to have a unique solution, it is necessary to impose a boundary condition on S_o. This boundary condition can always be expressed as

$$\hat{n} \times \left[\mu_r^{-1} \nabla \times \mathbf{E}(\mathbf{r},t)\right] + \gamma c^{-1} \hat{n} \times \partial_t \left[\hat{n} \times \mathbf{E}(\mathbf{r},t)\right] = 0 \quad \mathbf{r} \in S_o \tag{2}$$

where $\hat{n}$ represents the outward unit vector normal to S_o and γ is an unknown coefficient that depends on position and time. Obviously, (2) relates the tangential electric and magnetic fields on S_o. To evaluate γ, we introduce a fictitious source boundary S_s that resides inside S_o and also fully encloses the scatterer. On S_s, we define equivalent electric and magnetic currents as

$$\mathbf{J}(\mathbf{r},t) = -\hat{n} \times \left\{\mu^{-1} \partial_t^{-1} \left[\nabla \times \mathbf{E}(\mathbf{r},t)\right]\right\} \quad \mathbf{r} \in S_s \tag{3}$$

and

$$\mathbf{K}(\mathbf{r},t) = -\hat{n} \times \mathbf{E}(\mathbf{r},t) \quad \mathbf{r} \in S_s. \tag{4}$$

Here ∂_t^{-1} denotes temporal integration. These equivalent currents in turn define the electric and magnetic vector potentials

$$\mathbf{A}(\mathbf{r},t) = \mu_0 \iint_{S_s} \mathbf{J}(\mathbf{r}',t) \star g(|\mathbf{r}-\mathbf{r}'|,t)\, ds' \tag{5}$$

and

$$\mathbf{F}(\mathbf{r},t) = \epsilon_0 \iint_{S_s} \mathbf{K}(\mathbf{r}',t) \star g(|\mathbf{r}-\mathbf{r}'|,t)\, ds' \tag{6}$$

where $g(|\mathbf{r}-\mathbf{r}'|,t)$ denotes the 3-D Green's function

$$g(|\mathbf{r}-\mathbf{r}'|,t) = \frac{\delta\left(t - c^{-1}|\mathbf{r}-\mathbf{r}'|\right)}{4\pi|\mathbf{r}-\mathbf{r}'|}. \tag{7}$$

From the vector potentials $\mathbf{A}$ and $\mathbf{F}$, the temporal derivatives of the electric and magnetic fields on S_o can be computed as

$$\partial_t \mathbf{E}(\mathbf{r},t) = -\left(\partial_t^2 \mathcal{I} - c^2 \nabla\nabla\right) \cdot \mathbf{A}(\mathbf{r},t) - \frac{\partial_t}{\epsilon} \nabla \times \mathbf{F}(\mathbf{r},t) \quad \mathbf{r} \in S_o \tag{8}$$

$$\nabla \times \mathbf{E} = -\partial_t \nabla \times \mathbf{A}(\mathbf{r},t) + \mu\left(\partial_t^2 \mathcal{I} - c^2 \nabla\nabla\right) \cdot \mathbf{F}(\mathbf{r},t) \quad \mathbf{r} \in S_o \tag{9}$$

where $\mathcal{I}$ is the idempotent. These fields subsequently define the unknown coefficient γ.

In accordance with the variational principle [39], the solution to the boundary-value problem defined by (1) and (2) is obtained by seeking the stationary point of the functional

$$\begin{aligned} F\left[\mathbf{E}(\mathbf{r},t)\right] = & \frac{1}{2} \iiint_{V_o} \Big\{ \mu_r^{-1} \left[\nabla \times \mathbf{E}(\mathbf{r},t)\right] \cdot \left[\nabla \times \mathbf{E}(\mathbf{r},t)\right] \\ & + \mu_0 \epsilon \partial_t^2 \mathbf{E}(\mathbf{r},t) \cdot \mathbf{E}(\mathbf{r},t) \\ & + \sigma \mu_0 \partial_t \mathbf{E}(\mathbf{r},t) \cdot \mathbf{E}(\mathbf{r},t) \Big\} dv \\ & + \frac{1}{2} \iint_{S_o} \Big\{ \gamma c^{-1} \partial_t \left[\hat{n} \times \mathbf{E}(\mathbf{r},t)\right] \\ & \cdot \left[\hat{n} \times \mathbf{E}(\mathbf{r},t)\right] \Big\} ds. \end{aligned} \tag{10}$$

The FE discretization of (10) results in a matrix equation that contains γ. Since γ is a function of time, the system matrix must however be updated at every time step; this renders the scheme inefficient and unattractive.

Alternatively, one can replace (2) with

$$\hat{n} \times \left[\mu_r^{-1} \nabla \times \mathbf{E}(\mathbf{r},t)\right] = \mathbf{P}_S \quad \mathbf{r} \in S_o \tag{11}$$

where $\mathbf{P}_S$ is evaluated using a BI. In this case, the pertinent functional is

$$\begin{aligned} F\left[\mathbf{E}(\mathbf{r},t)\right] = & \frac{1}{2} \iiint_{V_o} \Big\{ \mu_r^{-1} \left[\nabla \times \mathbf{E}(\mathbf{r},t)\right] \cdot \left[\nabla \times \mathbf{E}(\mathbf{r},t)\right] \\ & + \mu_0 \epsilon \partial_t^2 \mathbf{E}(\mathbf{r},t) \cdot \mathbf{E}(\mathbf{r},t) \\ & + \sigma \mu_0 \partial_t \mathbf{E}(\mathbf{r},t) \cdot \mathbf{E}(\mathbf{r},t) \Big\} dv \\ & + \iint_{S_o} \mathbf{E}(\mathbf{r},t) \cdot \mathbf{P}_S ds. \end{aligned} \tag{12}$$

The resultant FE matrix is constant and does not need to be updated at every time step. However, since the evaluation of

the right-hand side of (11) involves only the magnetic field, the solution supports spurious modes whose frequencies correspond to the resonant frequencies of a cavity formed by covering S_o with perfect magnetically conducting walls while filling V_o with the exterior medium. These spurious modes creep into the solution throughout the time marching procedure and lead to instabilities.

Instead of specifying the tangential magnetic field on S_o as in (11), we may also specify the tangential electric field on S_o as

$$\hat{n} \times \mathbf{E}(\mathbf{r}, t) = \mathbf{Q}_S \tag{13}$$

where $\mathbf{Q}_S$ is evaluated using a BI. The required functional is still given by (12) but without the integral over S_o. However, since $\mathbf{Q}_S$ involves only the electric field, the solution supports spurious modes whose frequencies correspond to the resonant frequencies of a cavity formed by covering S_o with a perfect electric conductor while filling V_o with the exterior medium. Again, this leads to corruption of the desired solution and eventually to instabilities.

To eliminate these problems, we propose a novel scheme, which amounts to rewriting (2) in the form of the first-order impedance boundary condition as

$$\hat{n} \times \left[\mu_r^{-1} \nabla \times \mathbf{E}(\mathbf{r}, t)\right] + c^{-1} \hat{n} \times \partial_t \left[\hat{n} \times \mathbf{E}(\mathbf{r}, t)\right] = \mathbf{U}_S \quad \mathbf{r} \in S_o \tag{14}$$

where $\mathbf{U}_S$ is evaluated using a BI. Now, the pertinent functional becomes

$$\begin{aligned} F\left[\mathbf{E}(\mathbf{r}, t)\right] = & \frac{1}{2} \iiint_{V_o} \Big\{ \mu_r^{-1} \left[\nabla \times \mathbf{E}(\mathbf{r}, t)\right] \cdot \left[\nabla \times \mathbf{E}(\mathbf{r}, t)\right] \\ & + \mu_0 \epsilon \partial_t^2 \mathbf{E}(\mathbf{r}, t) \cdot \mathbf{E}(\mathbf{r}, t) \\ & + \sigma \mu_0 \partial_t \mathbf{E}(\mathbf{r}, t) \cdot \mathbf{E}(\mathbf{r}, t) \Big\} dv \\ & + \frac{1}{2} \iint_{S_o} \Big\{ c^{-1} \partial_t \left[\hat{n} \times \mathbf{E}(\mathbf{r}, t)\right] \cdot \left[\hat{n} \times \mathbf{E}(\mathbf{r}, t)\right] \\ & + 2 \mathbf{E}(\mathbf{r}, t) \cdot \mathbf{U}_S \Big\} ds. \end{aligned} \tag{15}$$

This formulation does not require the the FE matrix to be updated in each time step. In addition, our numerical experiments reveal that solutions obtained using this formulation are devoid of spurious modes. Interestingly, if the scattered component in $\mathbf{U}_S$ is set to zero, (14) becomes the first-order ABC. Evidently, the BI corrects this first-order condition so that (14) provides an exact ABC.

B. Numerical Discretization

To discretize (15), we first expand $\mathbf{E}$ as

$$\mathbf{E}(\mathbf{r}, t) = \sum_{i=1}^{N} u_i(t) \mathbf{N}_i(\mathbf{r}) \tag{16}$$

where N denotes the total number of expansion terms and $\mathbf{N}_i$ and u_i are the vector expansion functions and corresponding expansion coefficients, respectively. Substituting (16) into (15), taking the partial derivative of the functional with respect to the expansion coefficients u_i and setting the resultant equation to zero yields the following system of ordinary differential equations:

$$\mathbf{T} \frac{d^2 u}{dt^2} + (\mathbf{R} + \mathbf{Q}) \frac{du}{dt} + \mathbf{S} u + w = 0. \tag{17}$$

Here $\mathbf{T}$, $\mathbf{R}$, $\mathbf{Q}$, and $\mathbf{S}$ are square matrices and u and w are column vectors. Their elements are given by

$$\begin{aligned} \mathbf{T}_{ij} &= \mu_0 \epsilon \left\langle \mathbf{N}_i, \mathbf{N}_j \right\rangle_{V_o} \\ \mathbf{S}_{ij} &= \mu_r^{-1} \left\langle \nabla \times \mathbf{N}_i, \nabla \times \mathbf{N}_j \right\rangle_{V_o} \\ \mathbf{R}_{ij} &= \mu_0 \sigma \left\langle \mathbf{N}_i, \mathbf{N}_j \right\rangle_{V_o} \\ \mathbf{Q}_{ij} &= c^{-1} \left\langle \hat{n} \times \mathbf{N}_i, \hat{n} \times \mathbf{N}_j \right\rangle_{S_o} \\ w_i &= \left\langle \mathbf{N}_i, \mathbf{U}_S \right\rangle_{S_o} \end{aligned} \tag{18}$$

where $\langle \cdot, \cdot \rangle_{V_o}$ and $\langle \cdot, \cdot \rangle_{S_o}$ denote volume and surface integration, respectively.

Equation (17) can be discretized in time by many differencing schemes such as the central difference, the backward difference [30] and the Newmark method [29], [31], [40]. The latter two can yield unconditionally stable schemes, in which the time step is not constrained by the spatial discretization, but is limited by the accuracy requirement. The former yields a conditionally stable one, in which the time step requires to satisfy a certain criterion to ensure stability [41]. In this work, we employ the central difference.

Adopting a traditional central difference scheme to approximate the first- and second-order time derivatives in (17), we obtain

$$\begin{aligned} \mathbf{P} u^{n+1} = & \left(\frac{2}{\Delta t^2} \mathbf{T} - \mathbf{S} \right) u^n \\ & + \left[\frac{1}{2\Delta t} (\mathbf{R} + \mathbf{Q}) - \frac{1}{\Delta t^2} \mathbf{T} \right] u^{n-1} - w^n \end{aligned} \tag{19}$$

in which

$$\mathbf{P} = \frac{1}{\Delta t^2} \mathbf{T} + \frac{1}{2\Delta t} (\mathbf{R} + \mathbf{Q}) \tag{20}$$

and Δt represents the time step. Clearly, u^{n+1} can be solved for in a time marching fashion provided that w^n can be evaluated from $(u^1, \ldots, u^{n-1})$; a fast method for achieving this will be discussed in the next section.

It now remains to choose the $\mathbf{N}_i$. We implemented both zeroth- and higher-order schemes. In the zeroth-order FE method, we use the well-known edge-based vector basis functions defined in [24]. In the higher-order FE scheme, we employ the higher-order interpolatory vector basis functions defined in [42]. They are chosen because of their completeness and the availability of simple expressions for any order.

III. Boundary Integral Evaluation

To compute w^n at every time step, it is necessary to evaluate $\mathbf{U}_S$ in (14), which requires computation of a linear superposition of temporal derivatives of the electric and magnetic fields radiated by equivalent current sources $\mathbf{J}(\mathbf{r}, t)$ and $\mathbf{K}(\mathbf{r}, t)$ that reside on S_s. Evaluating these fields is tantamount to evaluating the potentials $\mathbf{A}(\mathbf{r}, t)$ and $\mathbf{F}(\mathbf{r}, t)$ by spatial and temporal convolutions of these currents with the Green's function. It is

well known that this evaluation is computationally expensive, a fact which has been one of the primary impediments to the popularity of the integral equation based transient analysis schemes. Indeed, if the duration of analysis is N_t time steps and the currents are represented using N_s functions, the cost of evaluating these fields/potentials scales as $\mathcal{O}(N_t N_s^2)$. In arriving at the above estimate, it has tacitly been assumed that the source and the observation surfaces are close to each other; therefore, the number of source and observation points are approximately equal. Recently, we introduced the PWTD algorithm. This scheme permits the fast evaluation of fields due to bandlimited sources and is the time domain counterpart of the frequency-domain fast multiple method. This scheme has been used for accelerating large-scale electromagnetic transient scattering analysis [43]. More recently, it has been used for accelerating global boundary condition kernels for truncating the computational domain of the FDTD solvers used for electromagnetic analysis [44]. In what follows, we shall detail the particulars of the scheme as it applies to accelerating the BIs required for truncating the time-domain FE method scheme.

Consider two equal size boxes denoted α_s and α_o. Assuming that α_s contains a collection of sources, our objective is to arrive at a plane wave representation of the vector potentials at locations in the observer box α_o. To this end, assume that the electric and magnetic currents that reside in α_s are represented as $\mathbf{J}^{\alpha_s}(\mathbf{r},t)=\sum_{n=1}^{N_{\alpha_s}}\mathbf{J}_n^{\alpha_s}(\mathbf{r},t)$, $\mathbf{K}^{\alpha_s}(\mathbf{r},t)=\sum_{n=1}^{N_{\alpha_s}}\mathbf{K}_n^{\alpha_s}(\mathbf{r},t)$, where N_{α_s} is the number of spatial discretization points for currents in α_s. Next, the temporal signatures of these current densities are divided into L consecutive subsignals each of duration T_s defined below as follows

$$\mathbf{J}_n^{\alpha_s}(\mathbf{r},t)=\sum_{l=1}^{L}\mathbf{J}_{nl}^{\alpha_s}(\mathbf{r},t) \tag{21}$$

$$\mathbf{K}_n^{\alpha_s}(\mathbf{r},t)=\sum_{l=1}^{L}\mathbf{K}_{nl}^{\alpha_s}(\mathbf{r},t) \tag{22}$$

where $\mathbf{J}_{nl}^{\alpha_s}(\mathbf{r},t)$ and $\mathbf{K}_{nl}^{\alpha_s}(\mathbf{r},t)$ are approximately bandlimited to $\omega_s=\pi/\Delta_t=\chi_1\omega_{\max}$ [14] with $\chi_1>1$ and of essential duration T_s. Dividing the source currents in this manner using a prolate series has been described elsewhere [16]. It has been demonstrated that if $R_c/c>T_s$, then the field in α_o due to sources in α_s can be reconstructed as a superposition of plane waves due to each subsignal [16], [43]. Using this source representation, it can be shown that the electric and magnetic vector potentials may be constructed as

$$\mathbf{\Psi}_{ml}(\mathbf{r},t)=\varpi\sum_{p=0}^{K}\sum_{q=-K}^{K}w_{pq}\left[\delta\left(t-\hat{k}_{pq}\cdot(\mathbf{r}-\mathbf{r}_m^c)\right)\right.$$
$$\left.{}^{*}\mathcal{T}\left(\hat{k}_{pq},t\right){}^{*}\mathcal{S}_n^{+}\left(\mathbf{I}_{nl},t\right)\right] \tag{23}$$

where (see (24) and (25) at the bottom of the page). In (23), $\mathbf{r}_s^c$ is used to denote the center of the box that either the source (n) or observer (m) resides in. Likewise, for any (n,m) $\{\varpi,\mathbf{I}_{nl}(\mathbf{r},t),\mathbf{\Psi}_{ml}(\mathbf{r},t)\}$ is either $\{\mu,\mathbf{J}_{nl}^{\alpha_s}(\mathbf{r},t),\mathbf{A}_{ml}^{\alpha_s}(\mathbf{r},t)\}$ or $\{\epsilon,\mathbf{K}_{nl}^{\alpha_s}(\mathbf{r},t),\mathbf{F}_{ml}(\mathbf{r},t)\}$, $K=\lceil 2\chi_1\chi_2R_s\omega_{\max}/c\rceil$, where $\chi_2>1$, $P_\upsilon(\cdot)$ is the Legendre polynomial of degree υ and $R_c=|\mathbf{R}_c|=|\mathbf{r}_m^c-\mathbf{r}_n^c|$. Equation (23) is valid after the source $\mathbf{I}_{nl}$ has stopped radiating. The potential $\mathbf{\Psi}_{ml}$ is a superposition of $\mathbf{\Psi}_{ml}^e$. Integration weights and plane wave directions necessary to evaluate (23) are given in [45]. Using the fact that for plane wave, the operator ∇ commutes with $-\hat{k}_{pq}\partial_t/c$ along with (8) and (9) permits the definitions of plane wave representations for the temporal derivatives of the electric and magnetic fields [43] and finally (see (26) at the bottom of the next page). As (26) indicates, $\langle\mathbf{N}_m,\mathbf{U}_S\rangle$ can be evaluated using a three-stage procedure. To arrive at a hierarchical computational scheme of reduced complexity, the entire computational domain is enclosed in a fictitious cubical box. This box is recursively divided N_l times. Any box is termed the *parent* box of the *children* that it is divided into. The fundamental signal duration $T_s(l)$ at any level is chosen proportional to the dimension of boxes at that level. Given this choice and in light of the arguments in the preceding paragraph regarding reconstruction of fields using a superposition of plane waves, the next task is to identify near- and far-field pairs at all levels. This is done using the following mechanism: at any level, members of a box pair are said to be in each other's far field if the distance between their closest points is greater than $cT_s(l)$ and the distance between the closest points of their parents is less than $cT_s(l+1)$. At the lowest level, all box pairs that are separated by a distance less than $cT_s(1)$ are said to be in each other's near field. Given this tree structure, the computation proceeds in two distinct stages: 1) the equivalent currents on S_s are computed at every time step and stored and the $\langle\mathbf{N}_i,\mathbf{U}\rangle_{S_o}$ for all i that belong in the near-field interaction list at the lowest level are computed; 2) Next, all interactions are computed using (26). Details

$$\mathcal{T}\left(\hat{k}_{pq},t\right)=\begin{cases}-\frac{\partial_t}{8\pi^2c}\sum_{\upsilon=1}^{K}(2\upsilon+1)P_\upsilon\left(\frac{ct}{R_c}\right)P_\upsilon\left(\hat{k}_{pq}\cdot\mathbf{R}_c\right), if|t|\le\frac{c}{R_c}\\ 0, \qquad \text{elsewhere}\end{cases} \tag{24}$$

and

$$\mathcal{S}_s^{\pm}\left(\mathbf{I}_s,t\right)=\iint_{S_s}\mathbf{I}_{sl}(\mathbf{r},t)\delta\left(t\pm\hat{k}_{pq}\cdot(\mathbf{r}-\mathbf{r}_s^c)\right)ds. \tag{25}$$

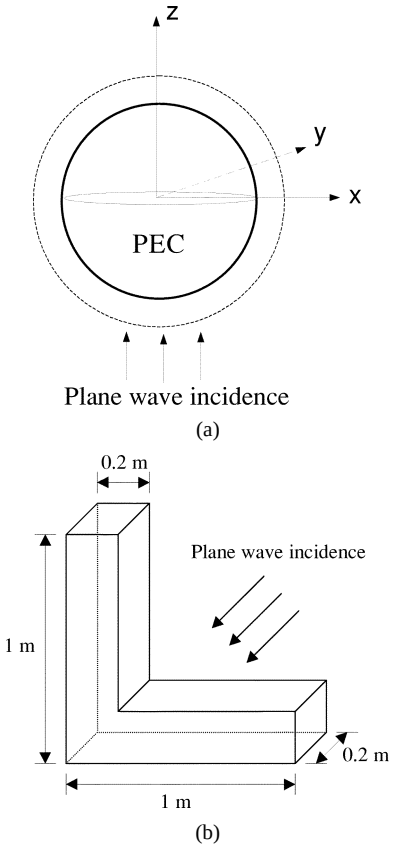

Fig. 2. (a) Conducting or dielectric-coated conducting sphere under the plane wave incidence. (b) An L-shaped stub under the plane wave incidence.

pertinent to the far field implementation of this algorithm can be found in [16], [17].

IV. Far-Field Computation

Once the electric and magnetic currents on the source boundary are obtained, the scattered field in the far-field zone can be evaluated via a far-field approximation. The scattered electric field at a far point $\mathbf{r}$ is given by

$$\begin{aligned} E_\theta^{\text{far}} =& -(4\pi rc)^{-1}\partial_t \\ &\cdot\left[L_\phi\left(\mathbf{r}, t-c^{-1}\hat{\mathbf{k}}\cdot\mathbf{r}\right)+\eta N_\theta\left(\mathbf{r}, t-c^{-1}\hat{\mathbf{k}}\cdot\mathbf{r}\right)\right] \\ E_\phi^{\text{far}} =&(4\pi rc)^{-1}\partial_t \\ &\cdot\left[L_\theta\left(\mathbf{r}, t-c^{-1}\hat{\mathbf{k}}\cdot\mathbf{r}\right)-\eta N_\phi\left(\mathbf{r}, t-c^{-1}\hat{\mathbf{k}}\cdot\mathbf{r}\right)\right] \end{aligned} \tag{27}$$

where $\mathbf{L}(\mathbf{r},\mathbf{t})$ and $\mathbf{N}(\mathbf{r},\mathbf{t})$ can be evaluated from the electric and magnetic currents $\mathbf{J}$ and $\mathbf{K}$ defined on S_s as

$$\begin{aligned} \mathbf{L}(\mathbf{r},t) &= \iint_{S_s}\mathbf{K}\left(\mathbf{r}', t+c^{-1}\hat{\mathbf{r}}\cdot\mathbf{r}'\right)ds' \\ \mathbf{N}(\mathbf{r},t) &= \iint_{S_s}\mathbf{J}\left(\mathbf{r}', t+c^{-1}\hat{\mathbf{r}}\cdot\mathbf{r}'\right)ds'. \end{aligned} \tag{28}$$

The above surface integrals are discretized in space using Gaussian quadrature. The discretized currents $\mathbf{J}$ and $\mathbf{K}$ are interpolated from the unknowns of the FE solution.

Once the scattered field in the far-field zone is known, the radar cross section (RCS) of the scatterer can be obtained from

$$\sigma = \lim_{r\to\infty} 4\pi r^2 \frac{\left|\mathcal{F}\left\{\mathbf{E}^{\text{far}}(\mathbf{r},t)\right\}\right|^2}{\left|\mathcal{F}\left\{\mathbf{E}^{\text{inc}}(\mathbf{r},t)\right\}\right|^2} \tag{29}$$

where $\mathcal{F}(\cdot)$ denotes the Fourier transform.

V. Numerical Examples

This section presents numerical examples to demonstrate the validity and performance of the proposed scheme. Two basic geometries are considered: one is a conducting or dielectric-coated conducting sphere for which the exact scattering solution is available in the form of a Mie series and the other is an L-shaped object, for which the FDTD solution is used as a reference. Both geometries are sketched in Fig. 2. For all examples considered herein, the incident wave is assumed to be a Neumann pulse, i.e., the time derivative of a Gaussian pulse

$$\begin{aligned} \mathbf{E}^{\text{inc}}(\mathbf{r},t) = \hat{\mathbf{E}}\Bigg\{ & 2\left[t-t_0-c^{-1}\hat{\mathbf{k}}\cdot(\mathbf{r}-\mathbf{r}_0)\right] \\ & \cdot\exp\left\{-\frac{\left[t-t_0-c^{-1}\hat{\mathbf{k}}\cdot(\mathbf{r}-\mathbf{r}_0)\right]^2}{\tau^2}\right\}\Bigg\}. \end{aligned} \tag{30}$$

Here, $\hat{\mathbf{k}}$ and $\hat{\mathbf{E}}$ denote the direction of propagation and polarization of the incident pulse, respectively and t_0, $\mathbf{r}_0$, and τ are parameters that define the pulse's temporal and spectral reference points and width. We also define $f_{\max}$ to be the frequency at which the amplitude of the pulse's spectrum decays to 10^{-10} times its peak value.

A. Zeroth-Order Results

The first example involves a perfect electrically conducting (PEC) sphere of radius 0.8 m. The computational domain is truncated by a spherical surface placed two elements away from the PEC surface and is discretized using 17 547 tetrahedra

$$\begin{aligned} \langle\mathbf{N}_m,\mathbf{U}_S\rangle =& \frac{1}{c^2}\sum_{p=0}^{K}\sum_{q=-K}^{K} w_{pq}\left[\mathcal{S}_m^-(\mathbf{N}_m,t)\times\hat{n}\times\hat{n}-\mathcal{S}_m^-(\mathbf{N}_m,t)\times\hat{n}\times\frac{\hat{k}_{pq}}{\mu}\right]^T * \partial_t^2\mathcal{T}\left(\hat{k}_{pq},t\right) \\ & * \left[\eta\hat{k}_{pq}\times\hat{k}_{pq}\times\mathcal{S}_n^+(\mathbf{J}_n,t)+\hat{k}_{pq}\times\mathcal{S}_n^+(\mathbf{K}_n,t)\right]. \end{aligned} \tag{26}$$

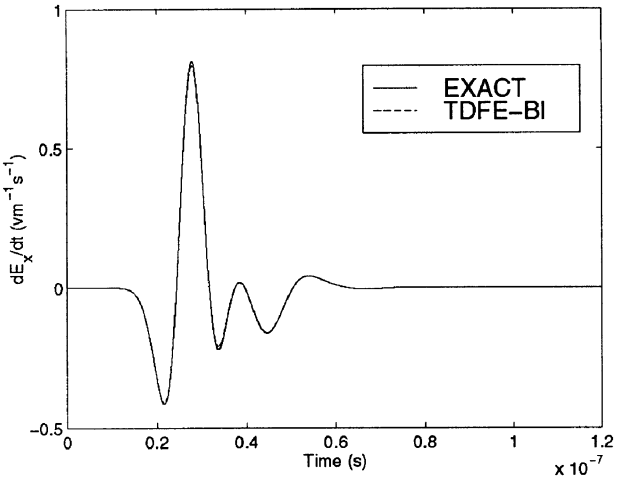

(a)

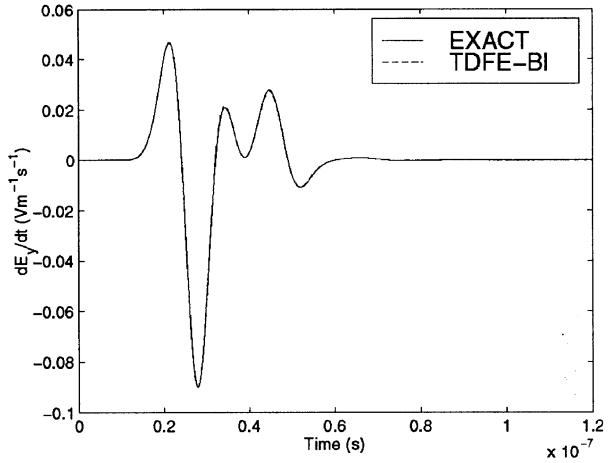

(b)

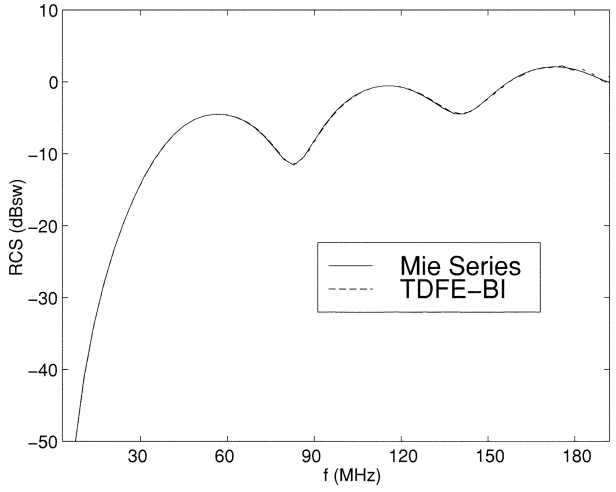

(c)

Fig. 3. Scattering by a conducting sphere. (a) Temporal derivative of E_x at observation point $\mathbf{r} = 0.33\hat{\mathbf{x}} - 1.03\hat{\mathbf{y}} - 0.45\hat{\mathbf{z}}$ m. (b) Temporal derivative of E_y at observation point $\mathbf{r} = -0.12\hat{\mathbf{x}} - 0.397\hat{\mathbf{y}} - 1.09\hat{\mathbf{z}}$ m. (c) RCS frequency response.

resulting in 23 838 unknowns. The pulse parameters are $\hat{\mathbf{k}} = \hat{\mathbf{z}}$, $\hat{\mathbf{E}} = \hat{\mathbf{x}}$, $t_0 = 25.99$ ns, $\mathbf{r}_0 = -1.2\hat{\mathbf{z}}$ m and $\tau = 5.25$ ns

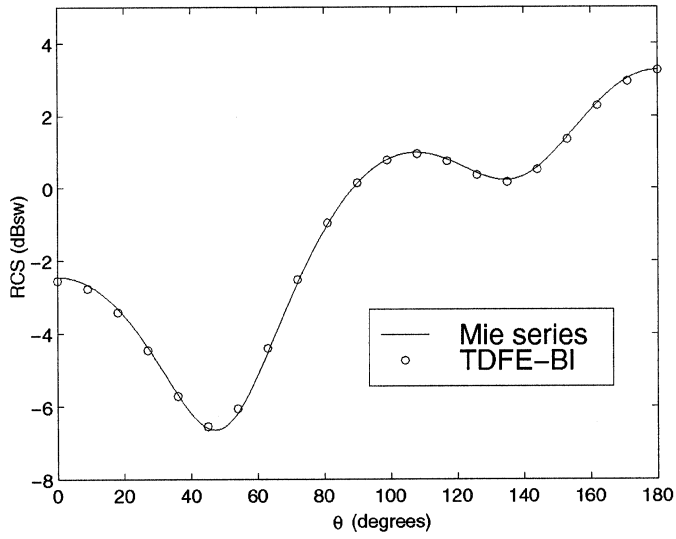

(a)

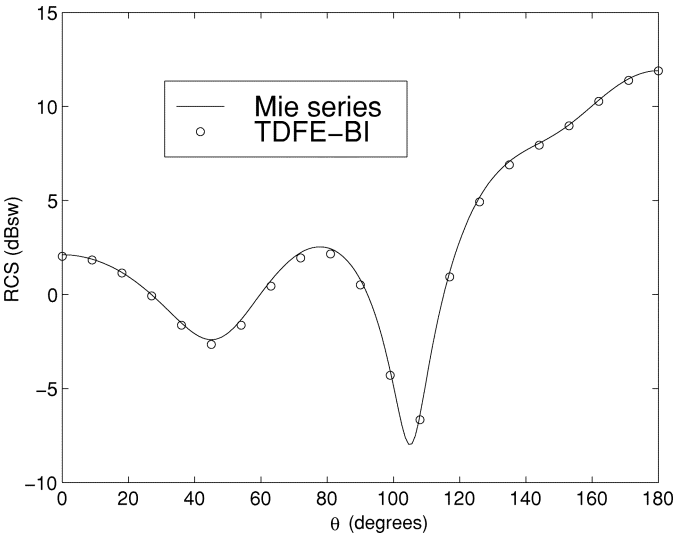

(b)

Fig. 4. E-plane bistatic RCS of a conducting sphere. (a) $f = 101.9$ MHz. (b) $f = 172.1$ MHz.

($f_{\max} = 300$ MHz). The source surface S_s is placed directly on the PEC surface. Fig. 3(a) and (b) show components of the total temporal electric fields at $\mathbf{r} = 0.33\hat{\mathbf{x}} - 1.03\hat{\mathbf{y}} - 0.45\hat{\mathbf{z}}$ m and $\mathbf{r} = -0.12\hat{\mathbf{x}} - 0.397\hat{\mathbf{y}} - 1.09\hat{\mathbf{z}}$ m, respectively. Excellent agreement is observed between the calculated and the exact results. Fig. 3(c) shows the backscatter RCS versus frequency and Fig. 4 depicts the bistatic RCS of the sphere at frequencies $f = 101.9$ MHz and $f = 172.1$ MHz.

The second example involves the L-shaped PEC object shown in Fig. 2(b). The parameters defining the incident pulse are $\hat{\mathbf{k}} = \cos(225^\circ)\hat{\mathbf{x}} + \sin(225^\circ)\hat{\mathbf{y}}$, $\hat{\mathbf{E}} = \cos(135^\circ)\hat{\mathbf{x}} + \sin(135^\circ)\hat{\mathbf{y}}$, $t_0 = 25.9$ ns, $\mathbf{r}_0 = 0.6\hat{\mathbf{x}} + 1.4\hat{\mathbf{y}}$ m and $\tau = 5.25$ ns ($f_{\max} = 300$ MHz). The mesh truncation surface is positioned two elements away from the object's surface. The simulation domain is subdivided into 42 601 tetrahedra, yielding 54 690 unknowns. The same problem is also analyzed using an FDTD solver which truncates the computational domain by a PML [46].

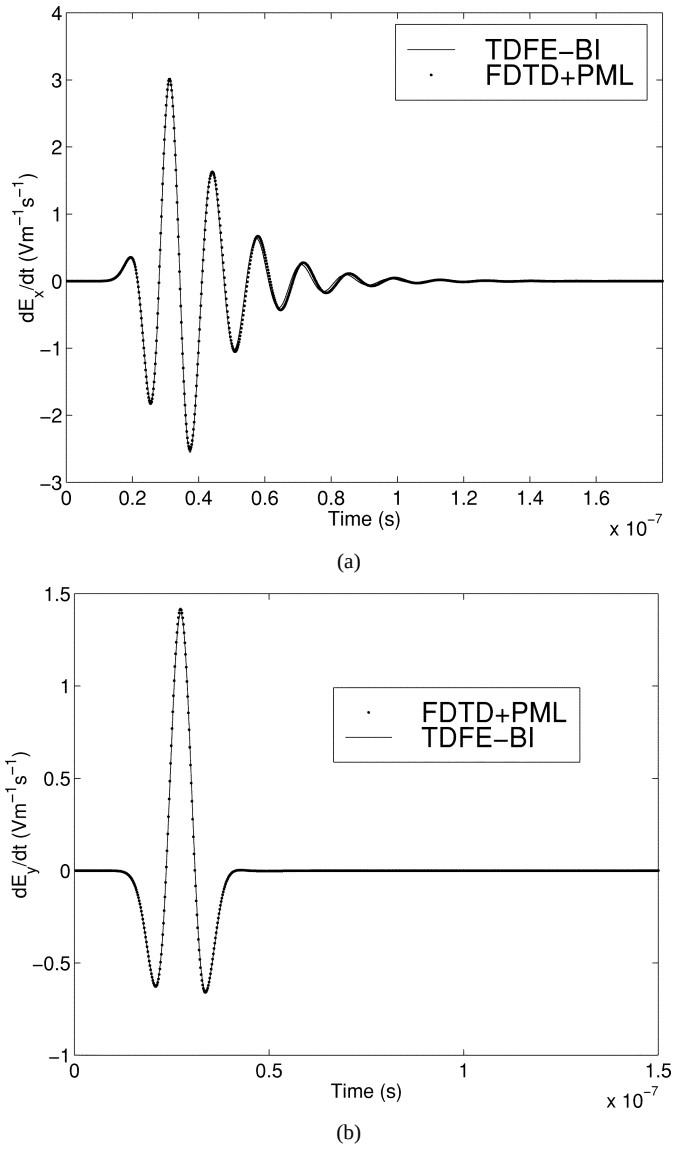

Fig. 5. (a) Scattering by a conducting L-shaped object at observation point $\mathbf{r} = 0.575\hat{\mathbf{x}} + 0.875\hat{\mathbf{y}} + 0.225\hat{\mathbf{z}}$ m. (b) Scattering by a dielectric L-shaped object at observation point $\mathbf{r} = 0.586\hat{\mathbf{x}} + 0.889\hat{\mathbf{y}} + 0.229\hat{\mathbf{z}}$ m.

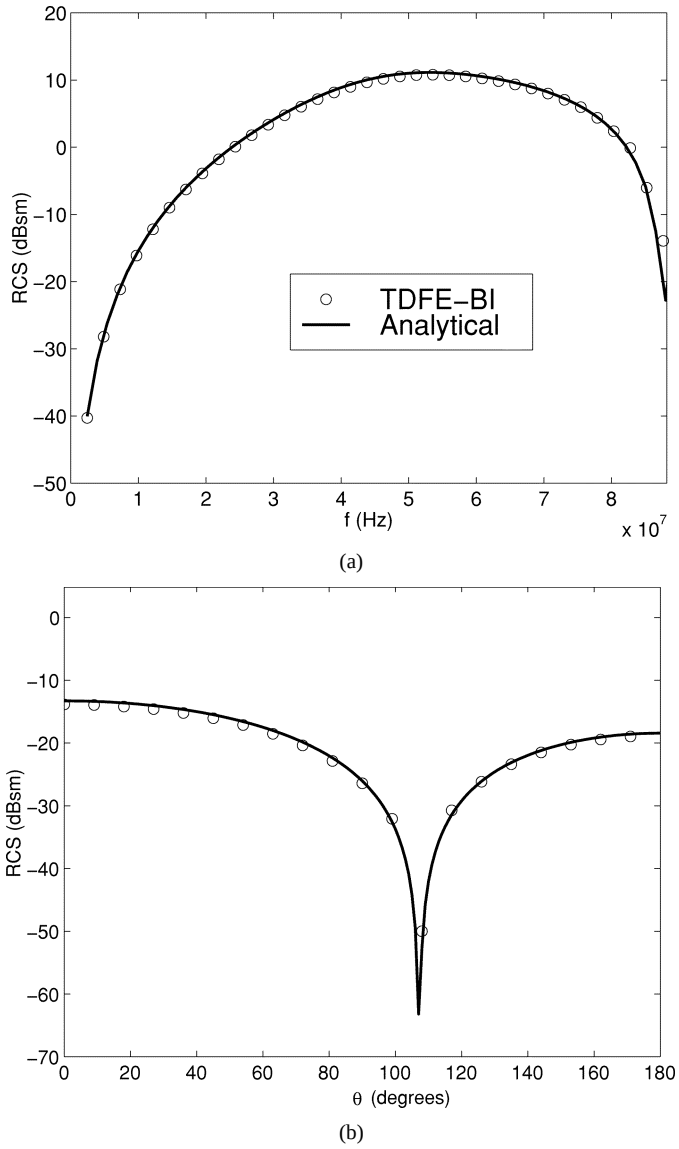

Fig. 6. RCS of a coated sphere with radius 1 m and $\epsilon_r = 4.0$. (a) Backscatter RCS. (b) Bistatic RCS at $f = 110$ MHz.

The use of the PML requires that the computational domain be a rectangular box since the PML cannot be applied to a concave outer surface; this, of course, artificially inflates the number of unknowns in the FDTD solver. The temporal signature of the electric field sampled at $\mathbf{r} = 0.575\hat{\mathbf{x}} + 0.875\hat{\mathbf{y}} + 0.225\hat{\mathbf{z}}$ m is shown in Fig. 5(a). The result obtained with the FE-BI scheme agrees very well with those obtained using the FDTD solver.

Next, to illustrate the capability of our algorithm to handle materials, we replace the L-shaped PEC object with a dielectric one. The dielectric has a relative permittivity of $\epsilon_r = 4.0$. The truncation surface is constructed in a manner similar to the above example. The computational region is discretized into 45 164 tetrahedra, generating 56 852 unknowns. The incident pulse is the same as in the previous example. Fig. 5(b) shows the temporal signature of components of the total electric field at $\mathbf{r} = 0.586\hat{\mathbf{x}} + 0.889\hat{\mathbf{y}} + 0.229\hat{\mathbf{z}}$ m, calculated with the FE-BI and FDTD solvers. Very good agreement between both sets of results is observed.

Finally, a coated sphere with radius of 1 m is considered. The dielectric coating has a thickness of 0.2 m and a relative permittivity of $\epsilon_r = 4.0$. The computational region is subdivided into 12 351 tetrahedra, yielding 16 047 unknowns. The Neumann pulse is defined by $t_0 = 51.99$ ns, $\mathbf{r}_0 = 1.2\hat{\mathbf{x}} + 1.2\hat{\mathbf{y}}$ m and $\tau = 10.5$ ns ($f_{\max} = 150$ MHz). Computed frequency domain RCS signatures are compared to the exact data in Fig. 6.

B. Higher-Order Results

When higher-order FEs are used, it is found that the condition number of the $\mathbf{P}$ matrix (19) grows rapidly and that the CG solver with a simple diagonal preconditioner converges slowly. Although this problem can be mitigated by using a better preconditioner, in this work, we employ an advanced direct sparse matrix solver that uses the multifrontal method [47]–[49]. The multifrontal method factorizes a large sparse matrix using a sequence of small dense frontal matrices. The square frontal matrices are factorized efficiently using dense

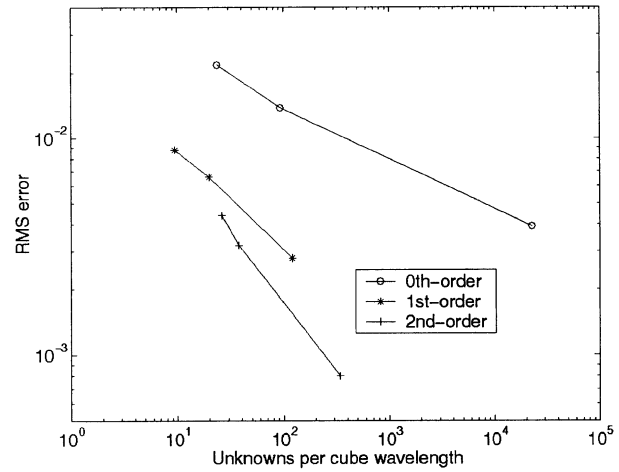

(a)

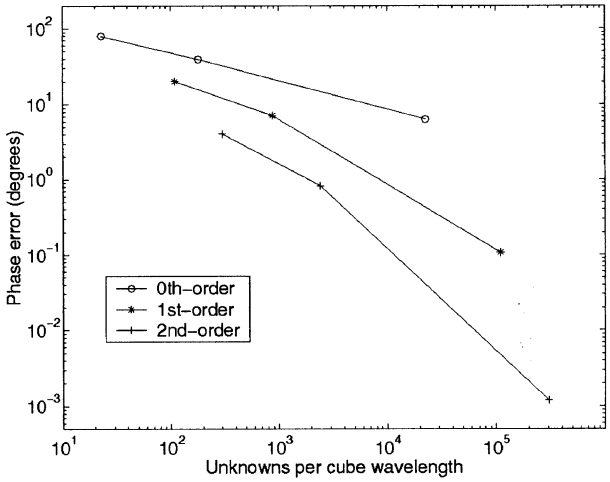

(b)

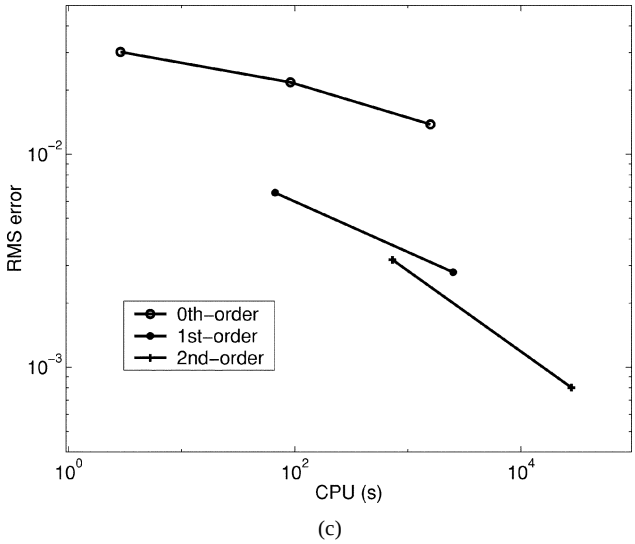

(c)

Fig. 7. (a) RMS error versus unknowns per cube wavelength. (b) Phase error versus unknowns per cube wavelength. (c) RMS error versus CPU time.

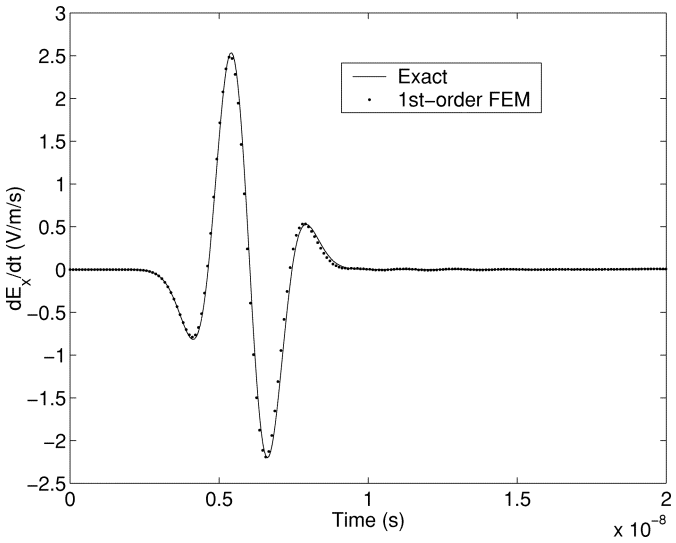

(a)

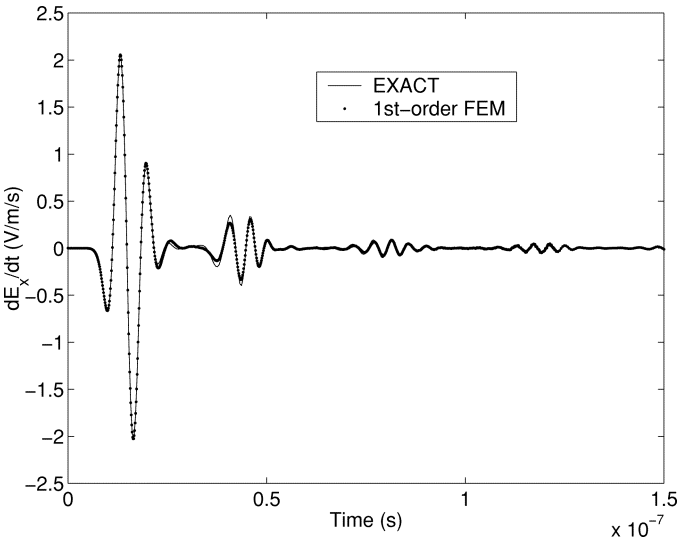

(b)

Fig. 8. (a) Scattering from a conducting sphere of dimension $10\lambda_{\min}$. (b) Scattering from a coated sphere of dimension $4\lambda_{\min}$.

matrix kernels. Since the method uses a sparse memory storage scheme, relatively large problems can be handled using readily available computer resources. Note that the factorization is performed only once and after that only forward and backward substitutions are needed in each time step.

To illustrate the advantages of the higher-order time-domain finite-element method (TDFEM), we consider a PEC sphere of radius 1 m. The incident pulse is characterized by $\hat{\mathbf{k}} = \hat{\mathbf{z}}, \hat{\mathbf{E}} = \hat{\mathbf{x}}$, $t_0 = 5.2$ ns, $\mathbf{r}_0 = -1.0\hat{\mathbf{z}}$ m and $\tau = 1.05$ ns; this pulse has a maximum frequency of 1.5 GHz or equivalently, a minimal wavelength $\lambda_{\min} = 0.2$ m. Three meshes are generated with the average edge length of the tetrahedra equal to $0.1\lambda_{\min}$, $0.5\lambda_{\min}$ and $1\lambda_{\min}$, respectively. For each mesh, calculations are carried out using zeroth-, first-, and second-order vector basis functions. The root-mean-square (RMS) error (normalized by the maximum amplitude) of the x-component of the electric field observed at $\mathbf{r} = 0.9\hat{\mathbf{x}} + 0.01\hat{\mathbf{y}} + 0.1\hat{\mathbf{z}}$ m is plotted as a function of the unknown density in Fig. 7(a). The higher-order accuracy and convergence due to the use of the higher-order basis functions are evident. In addition to the RMS error, it is also important

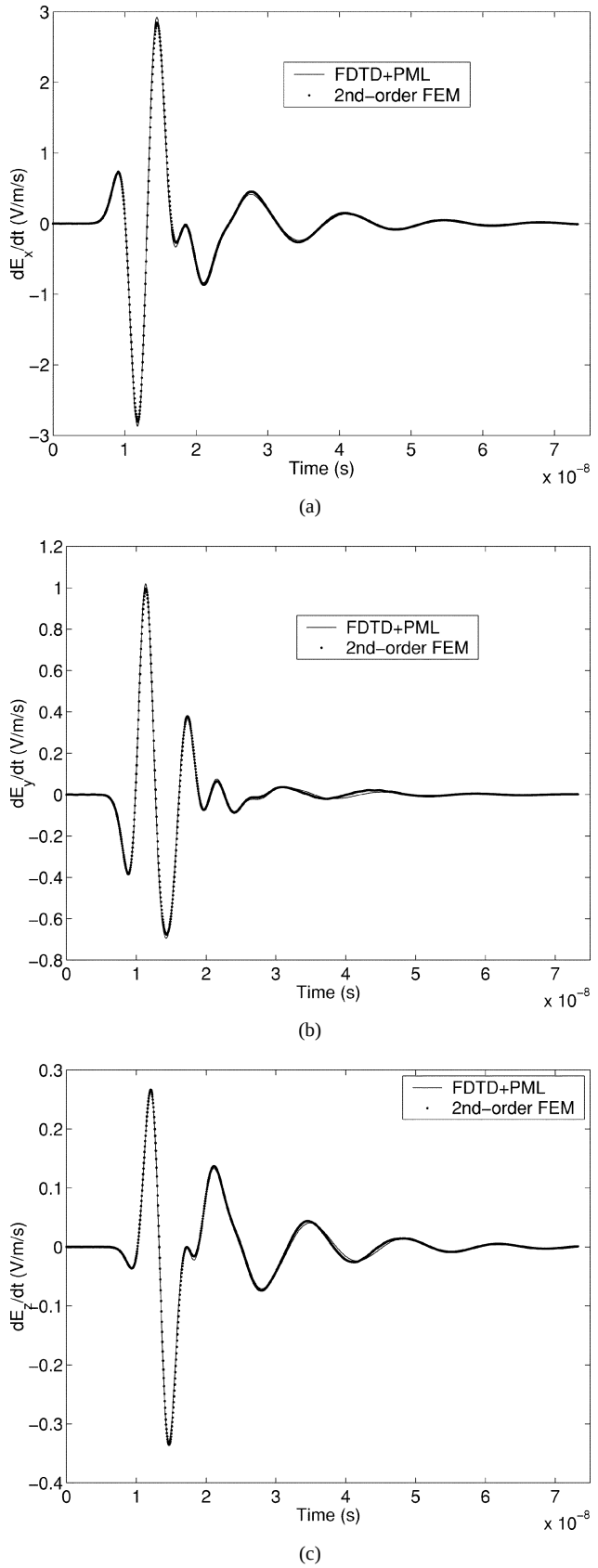

Fig. 9. Scattering from an L-shaped conducting object with electric size $5\lambda_{\min}$, observed at $\mathbf{r} = 0.55\hat{\mathbf{x}} + 0.89\hat{\mathbf{y}} + 0.25\hat{\mathbf{z}}$ m.

to examine the phase error that accumulates as the wave propagates through a large region or over a long period of time. It is well known that phase error accumulation using zeroth-order FE schemes severely impedes the analysis of late time responses. The problem is mitigated by the use of higher-order elements. Fig. 7(b) shows the phase error in the same calculations as described above. Again, it is clear that higher-order basis functions can significantly reduce the error at a much higher rate than the zeroth-order basis. Finally, Fig. 7(c) plots the RMS error as a function of the computing time to illustrate the better efficiency of the higher-order implementation.

Because of the superior accuracy and efficiency of the higher-order TDFEM, we can now analyze scattering from an electrically larger problem. Fig. 8(a) depicts the temporal derivative of the x-component of the electric field at $\mathbf{r} = 0.9\hat{\mathbf{x}} + 0.01\hat{\mathbf{y}} + 0.1\hat{\mathbf{z}}$ m in the presence of a PEC sphere of radius of 1 m. The incident Neumann pulse is defined by $\hat{\mathbf{k}} = \hat{\mathbf{z}}$, $\hat{\mathbf{E}} = \mathbf{x}$, $t_0 = 5.2$ ns, $\mathbf{r}_0 = -1.2\hat{\mathbf{z}}$ m and $\tau = 1.05$ ns ($f_{\max} = 1.5$ GHz). The results are obtained using the first-order finite-element method (FEM) with 4307 tetrahedra and 30 738 unknowns. Next, we consider the coated sphere shown in Fig. 2(a), which is also considered in the example that led to Fig. 6. The parameters for the incident pulse are also the same as in that example except that now $t_0 = 12.99$ ns and $\tau = 2.6$ ns ($f_{\max} = 0.6$ GHz). Fig. 8(b) shows the temporal derivative of the x-component of the electric field at $\mathbf{r} = 0.01\hat{\mathbf{y}} - 1.1\hat{\mathbf{z}}$ m. The results are obtained using the first-order FEM with 6815 tetrahedra and 46 942 unknowns. The effect of the creeping waves traveling around the surface is clearly seen in the figure.

Finally, we consider the L-shaped PEC object illustrated in Fig. 2(b). The incident Neumann pulse has the same parameters as the one used in the example of Fig. 5(a), except that now $t_0 = 5.2$ ns and $\tau = 1.05$ ns, which raises the maximum frequency to 1.5 GHz and reduces the minimum wavelength to $\lambda_{\min} = 0.2$ m. The simulation domain is subdivided into 5278 tetrahedra, yielding 106 266 unknowns for the second-order elements. The temporal electric fields sampled at $\mathbf{r} = 0.55\hat{\mathbf{x}} + 0.89\hat{\mathbf{y}} + 0.25\hat{\mathbf{z}}$ m are shown in Fig. 9. The results are compared with those obtained from the FDTD solver.

Although the above results are generated using up to the second-order basis functions, the code implemented is general and suitable for the use of any orders. However, as demonstrated clearly in Fig. 7, the largest increase of the accuracy comes from jumping from the zeroth-order basis to the first-order basis.

VI. Conclusion

A novel TD hybrid FE-BI method for analyzing open-region electromagnetic transient scattering problems was presented. The method uses an artificial boundary to truncate the infinite computational domain. A novel numerically exact absorbing condition that preserves the sparsity of the FE matrix and yields solutions free of spurious modes, was implemented, using higher-order vector basis functions defined on higher-order curvilinear elements. The PWTD algorithm was employed to efficiently evaluate the boundary integrals. The accuracy and versatility of the technique were demonstrated by several numerical examples.

REFERENCES

[1] P. P. Silvester and G. Pelosi, *Finite Elements for Wave Electromagnetics*. Piscataway, NJ: IEEE Press, 1994.

[2] K. S. Yee, "Numerical solution of initial boundary value problems involving Maxwell's equations in isotropic media," *IEEE Trans. Antennas Propagat.*, vol. AP–14, pp. 302–307, Mar. 1966.

[3] C. L. Bennet, "A Technique for Computing Approximate Impulse Response for Conducting Bodies," Ph.D. dissertation, Purdue Univ., West Lafayette, IN, 1968.

[4] R. Mittra, "Integral equation methods for transient scattering," in *Transient Electromagnetic Fields*, L. B. Felsen, Ed. New York: Springer-Verlag, 1976, ch. 2.

[5] A. G. Tijhuis, *Electromagnetic Inverse Profiling*. Utrecht, Netherlands: VNU, 1987.

[6] S. M. Rao and D. R. Wilton, "Transient scattering by conducting surfaces of arbitrary shape," *IEEE Trans. Antennas Propagat.*, vol. 39, pp. 56–61, Jan. 1991.

[7] B. P. Rynne and P. D. Smith, "Stability of time marching algorithms for the electric field integral equations," *J. Electromagn. Waves Applicat.*, vol. 12, pp. 1181–1205, 1990.

[8] P. D. Smith, "Instabilities in time marching methods for scattering: Cause and rectification," *Electromagn.*, vol. 10, pp. 439–451, 1990.

[9] D. A. Vechinski and S. M. Rao, "A stable procedure to calculate the transient scattering by conducting surfaces of arbitrary shape," *IEEE Trans. Antennas Propagat.*, vol. 40, pp. 661–665, June 1992.

[10] B. P. Rynne, "Stability and convergence of time marching methods in scattering problems," *Int. J. Appl. Math.*, vol. 35, pp. 297–310, 1985.

[11] M. J. Bluck and S. P. Walker, "Time-domain BIE analysis of large three dimensional electromagnetic scattering problems," *IEEE Trans. Antennas Propagat.*, vol. 45, pp. 894–901, May 1997.

[12] G. Manara, A. Monorchio, and R. Reggiannini, "A space-time discretization criterion for a stable time-marching solution of the electric field integral equation," *IEEE Trans. Antennas Propagat.*, vol. 45, pp. 527–532, Mar. 1997.

[13] S. M. Rao and T. K. Sarkar, "An efficient method to evaluate the time-domain scattering from arbitrarily shaped conducting bodies," *Microwave Opt. Technol. Lett.*, vol. 17, pp. 321–325, 1998.

[14] A. A. Ergin, B. Shanker, and E. Michielssen, "Fast evaluation of transient wave fields using diagonal translation operators," *J. Comp. Phys.*, vol. 146, pp. 157–180, 1998.

[15] S. P. Walker, "Scattering analysis via time-domain integral equations: Methods to reduce the scaling of cost with frequency," *IEEE Antennas Propagat. Mag.*, vol. 39, pp. 13–20, Oct. 1997.

[16] A. A. Ergin, B. Shanker, and E. Michielssen, "The plane wave time domain algorithm for the fast analysis of transient wave phenomena," *IEEE Antennas Propagat. Mag.*, vol. 41, no. 4, pp. 39–52, Aug. 1999.

[17] B. Shanker, A. A. Ergin, K. Aygün, and E. Michielssen, "The multilevel plane wave time domain algorithm for the fast analysis of transient scattering phenomena," in *Proc. IEEE Antennas Propagat. Soc.*, vol. 2, Orlando, FL, July 1999, pp. 1342–1346.

[18] A. C. Cangellaris, C. C. Lin, and K. K. Mei, "Point-matched time-domain finite element methods for electromagnetic radiation and scattering," *IEEE Trans. Antennas Propagat.*, vol. 35, pp. 1160–1173, Oct. 1987.

[19] J. T. Elson, H. Sangani, and C. H. Chan, "An explicit time-domain method using three-dimensional Whitney elements," *Microwave Opt. Technol. Lett.*, vol. 7, pp. 607–610, 1994.

[20] T. V. Yioultsis, N. V. Kantartzis, C. S. Antonopoulos, and T. D. Tsiboukis, "A fully explicit Whitney element-time domain scheme with higher order vector finite elements for three-dimensional high frequency problems," *IEEE Trans. Magn.*, vol. 34, pp. 3288–3291, 1998.

[21] M. Feliani and F. Maradei, "Hybrid finite element solution of time dependent Maxwell's curl equations," *IEEE Trans. Magn.*, vol. 31, pp. 1330–1335, May 1995.

[22] K. Choi, S. J. Salon, K. A. Connor, L. F. Libelo, and S. Y. Hahn, "Time domain finite element analysis of high power microwave aperture antennas," *IEEE Trans. Magn.*, vol. 31, pp. 1622–1625, May 1995.

[23] M. Hano and T. Itoh, "Three-dimensional time-domain method for solving Maxwell's equations based on circumference of elements," *IEEE Trans. Magn.*, vol. 32, pp. 946–949, May 1996.

[24] A. Bossavit and I. Mayergoyz, "Edge elements for scattering problems," *IEEE Trans. Magn.*, vol. 25, pp. 2816–2821, July 1989.

[25] M. F. Wong, O. Picon, and V. F. Hanna, "A finite-element method based on Whitney forms to solve Maxwell equations in the time-domain," *IEEE Trans. Magn.*, vol. 31, pp. 1618–1621, May 1995.

[26] K. Mahadevan and R. Mittra, "Radar cross section computation of inhomogeneous scatterers using edge-based finite element methods in frequency and time domains," *Radio Sci.*, vol. 28, pp. 1181–1193, Nov.–Dec. 1993.

[27] D. R. Lynch and K. D. Paulsen, "Time-domain integration of the Maxwell equations on finite elements," *IEEE Trans. Antennas Propagat.*, vol. 38, pp. 1933–1942, Dec. 1990.

[28] G. Mur, "The finite-element modeling of three-dimensional time-domain electromagnetic fields in strongly inhomogeneous media," *IEEE Trans. Magn.*, vol. 28, pp. 1130–1133, Mar. 1992.

[29] J. F. Lee and Z. Sacks, "Whitney elements time domain (WETD) methods," *IEEE Trans. Magn.*, vol. 31, pp. 1325–1329, May 1995.

[30] J. F. Lee, "WETD-a finite-element time-domain approach for solving Maxwell's equations," *IEEE Microwave Guided Wave Lett.*, vol. 4, pp. 11–13, Jan. 1994.

[31] S. D. Gedney and U. Navsariwala, "An unconditionally stable finite-element time-domain solution of the vector wave equation," *IEEE Microwave Guided Wave Lett.*, vol. 5, pp. 332–334, May 1995.

[32] D. A. White, "Orthogonal vector basis functions for time domain finite element solution of the vector wave equation," *IEEE Trans. Magn.*, vol. 35, pp. 1458–1461, May 1999.

[33] J. M. Jin, M. Zunoubi, K. C. Donepudi, and W. C. Chew, "Frequency-domain and time-domain finite-element solution of Maxwell's equations using spectral Lanczos decomposition method," *Comput. Methods Appl. Mech. Engr.*, vol. 169, pp. 279–296, 1999.

[34] J. F. Lee, R. Lee, and A. C. Cangellaris, "Time-domain finite element methods," *IEEE Trans. Antennas Propagat.*, vol. 45, pp. 430–442, Mar. 1997.

[35] J. R. Brauer, R. Mittra, and J. F. Lee, "Absorbing boundary condition for vector and scalar potentials arising in electromagnetic finite element analysis in frequency and time domains," in *Proc. IEEE Antennas Propagat. Soc. Int. Symp. Dig.*, ON, Canada, June 1991, pp. 1224–1227.

[36] K. Mahadevan, R. Mittra, D. Rowse, and J. Murphy, "Edge-based finite element frequency and time domain algorithms for RCS computation," in *Proc. IEEE Antennas Propagat Soc. Int. Symp. Dig.*, vol. 3, 1993, pp. 1680–1683.

[37] T. Roy, T. K. Sarkar, A. R. Djordjevic, and M. Salazar-Palma, "Time-domain analysis of TM scattering from conducting cylinders using a hybrid method," *IEEE Trans. Microwave Theory Tech.*, vol. 46, pp. 1471–1477, Oct. 1998.

[38] D. Jiao, M. Lu, E. Michielssen, and J. M. Jin, "A fast time-domain finite element-boundary integral method for electromagnetic analysis," IEEE Trans. Antennas Propagat., vol. 49, pp. 1453–1461, Oct. 2000, submitted for publication.

[39] J. M. Jin, *The Finite Element Method in Electromagnetics*. New York: Wiley, 1993.

[40] W. P. Carpes Jr., L. Pichon, and A. Razek, "A 3D finite element method for the modeling of bounded and unbounded electromagnetic problems in the time domain," *Int. J. Numer. Model.*, vol. 13, pp. 527–540, 2000.

[41] D. Jiao and J. M. Jin, "A general approach for the stability analysis of the time-domain finite-element method," in *Proc. IEEE Antennas Propagat. Soc. Int. Symp. Dig.*, vol. 4, Boston, MA, July 2001, pp. 506–509.

[42] R. D. Graglia, D. R. Wilton, and A. F. Peterson, "Higher order interpolatory vector bases for computational electromagnetics," *IEEE Trans. Antennas Propagat.*, vol. 45, pp. 329–341, Mar. 1997.

[43] B. Shanker, A. A. Ergin, K. Aygün, and E. Michielssen, "Computation of transient scattering from electrically large scatterers using the plane wave time domain algorithm," in *Proc. IEEE Antennas Propagat. Soc. Int. Symp. Dig.*, vol. 2, Atlanta, GA, June 1998, pp. 948–951.

[44] B. Shanker, A. A. Ergin, and E. Michielssen, "Plane-wave time-domain acceleration of exact radiation boundary conditions in FDTD analysis of electromagnetic phenomena," IEEE Trans. Antennas and Propagat., 2000, submitted for publication.

[45] B. Shanker, A. A. Ergin, K. Aygün, and E. Michielssen, "Analysis of transient electromagnetic scattering phenomena using a two-level plane wave time domain algorithm," *IEEE Trans. Antennas Propagat.*, vol. 48, pp. 510–523, Apr. 2000.

[46] C. E. Reuter, E. T. Thiele, and A. Taflove, "Validation and extension to three-dimensions of the Berenger PML absorbing boundary condition for FDTD meshes," *IEEE Microwave Guided Wave Lett.*, vol. 4, pp. 268–270, Aug. 1994.

[47] P. R. Amestoy and I. S. Duff, "Vectorization of a multiprocessor multifrontal code," *Int. J. Supercomput. Appl.*, vol. 3, pp. 41–59, 1989.

[48] T. A. Davis and I. S. Duff, "An unsymmetric-pattern multifrontal methods for parallel sparse LU factorization," *SIAM J. Matrix Anal. Appl.*, vol. 18, no. 1, pp. 140–158, 1997.
[49] J. W. H. Liu, "The multifrontal method for sparse matrix solution: Theory and practice," *SIAM Rev.*, vol. 34, pp. 82–109, 1992.

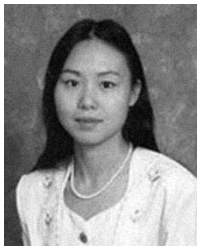

Dan Jiao (S'00–M'02) received the B.S. and M.S. degrees in electrical engineering from Anhui University, China, in 1993 and 1996, respectively. She is currently working toward the Ph.D. degree in electrical engineering at the University of Illinois at Urbana-Champaign.

From 1996 to 1998, she performed graduate studies at the University of Science and Technology of China, Hefei, China. Since 1998, she has been a Research Assistant at the Center for Computational Electromagnetics, University of Illinois at Urbana-Champaign. She has published over 20 papers in refereed journals and one book chapter. Her current research interests include fast computational methods in electromagnetics and time-domain numerical techniques.

Ms. Jiao was the recipient of the 2000 Raj Mittra Outstanding Research Award presented by the Department of Electrical and Computer Engineering, University of Illinois at Urbana-Champaign.

A. Arif Ergin received the Ph.D degree from the University of Illinois at Urbana-Champaign in 2000.

He is an Assistant Professor at the Gebze Institute of Technology, Kocaeli, Turkey. His current research interests include computational methods for analyzing wave propagation and scattering in acoustics and electromagnetics, antenna design and measurements, and electromagnetic compatability.

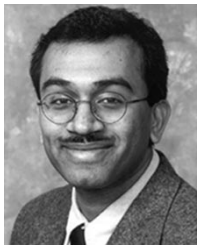

Balasubramaniam Shanker (M'96–SM'00) received the B.Tech from the Indian Institute of Technology, Madras, in 1989, and the M.S. and Ph.D degrees from Pennsylvania State University, University Park, in 1992 and 1993, respectively.

From 1993 to 1996, he was a Research Associate in the Department of Biochemistry and Biophysics at Iowa State University where he worked on molecular theory of optical activity. From 1996 to 1999, he was with the Center for Computational Electromagnetics at the University of Illinois, Urbana-Champaign. Currently, he is an Assistant Professor in the Electrical and Computer Engineering Department, Iowa State University, Ames. He has published over 45 journal articles and presented over 80 papers at conferences. His research interests include all aspects of computational electromagnetics and electromagnetic wave propagation in complex media.

Dr. Shanker is a Full Member of the USNC-URSI Commission B.

Eric Michielssen (M'95–SM'99–F'02) received the M.S. degree in electrical engineering (*summa cum laude*) from the Katholieke Universiteit Leuven (KUL), Belgium, and the Ph.D. degree in electrical engineering from the University of Illinois at Urbana-Champaign (UIUC) in 1987 and 1992, respectively.

From 1987 to 1988, he was a Research and Teaching Assistant with the Microwaves and Lasers Laboratory at KUL, and from 1988 to 1992, he was with the Electromagnetic Communication Laboratory at UIUC. In 1992, he joined the Faculty at the Department of Electrical and Computer Engieering where in 1998, he was promoted to Associate Professor. Since 1995, he has also served as Associate Director of the Center for Computational Electromagnetics at UIUC. He has authored or coauthored over 70 journal papers and book chapters and over 100 papers in conference proceedings. His research interests include all aspects of theoretical and applied computational electromagnetics. His principal research focus has been on the development of fast frequency and time domain integral-equation-based techniques for analyzing electromagnetic phenomena and the development of robust, genetic algorithm driven optimizers for the synthesis of electromagnetic and optical devices.

Dr. Michielssen received a Belgian American Educational Foundation Fellowship in 1988 and a Schlumberger Fellowship in 1990. He was the recipient of a 1994 International Union of Radio Scientists (URSI) Young Scientist Fellowship, a 1995 National Science Foundation CAREER Award and the 1998 Applied Computational Electromagnetics Society (ACES) Valued Service Award. He was also named 1999 URSI United States National Committee Henry G. Booker Fellow and selected as the recipient of the 1999 URSI Koga Gold Medal. Recently, he was awarded the UIUC's 2001 Xerox Award for Faculty Research and appointed Beckman Fellow in its Center for Advanced Studies. He served as the Technical Chairman of the 1997 Applied Computational Electromagnetics Society (ACES) Symposium (review of progress in applied computational electromagnetics, March 1997, Monterey, CA) and from 1998 to 2001, served on the ACES Board of Directors and as ACES Vice President. From 1997 to 1999, he was as an Associate Editor for *Radio Science* and he currently is an Associate Editor for the IEEE TRANSACTIONS ON ANTENNAS AND PROPAGATION. He is a Member of URSI Commission B.

Jian-Ming Jin (S'87–M'89–SM'94–F'01) received the B.S. and M.S. degrees in applied physics from Nanjing University, Nanjing, China, and the Ph.D. degree in electrical engineering from the University of Michigan, Ann Arbor, in 1982, 1984, and 1989, respectively.

He is a Full Professor in the Department of Electrical and Computer Engineering and Associate Director of the Center for Computational Electromagnetics at the University of Illinois at Urbana-Champaign. He has authored or coauthored over 110 papers in refereed journals and 15 book chapters. He has also authored *The Finite Element Method in Electromagnetics* (New York: Wiley, 1993) and *Electromagnetic Analysis and Design in Magnetic Resonance Imaging* (Boca Raton, FL: CRC, 1998), coauthored *Computation of Special Functions* (New York: Wiley, 1996), and coedited *Fast and Efficient Algorithms in Computational Electromagnetics* (Norwood, MA: Artech, 2001). His current research interests include computational electromagnetics, scattering and antenna analysis, electromagnetic compatibility and magnetic resonance imaging. He currently serves as an Associate Editor of *Radio Science* and is also on the Editorial Board for *Electromagnetics Journal* and *Microwave and Optical Technology Letters*.

Dr. Jin is a Member of Commission B of USNC/URSI, Tau Beta Pi, and the International Society for Magnetic Resonance in Medicine. He was a recipient of the 1994 National Science Foundation Young Investigator Award and the 1995 Office of Naval Research Young Investigator Award. He also received the 1997 Xerox Junior Research Award and the 2000 Xerox Senior Research Award presented by the College of Engineering, University of Illinois at Urbana-Champaign and was appointed as the first Henry Magnuski Outstanding Young Scholar in the Department of Electrical and Computer Engineering in 1998. His name is also often listed in the University of Illinois at Urbana-Champaign's *List of Excellent Instructors.* He was a Distinguished Visiting Professor in the Air Force Research Laboratory in 1999. He served as an Associate Editor of the IEEE TRANSACTIONS ON ANTENNAS and PROPAGATION from 1996 to 1998. He was the symposium Co-Chairman and Technical Program Chairman of the Annual Review of Progress in Applied Computational Electromagnetics in 1997 and 1998, respectively.